BASIC SCIENCE

Nanomedicine: Nanotechnology, Biology, and Medicine
13 (2017) 1645–1652

Original Article

nanomedjournal.com

# The effects of gold nanoparticles functionalized with β-amyloid specific peptides on an *in vitro* model of blood–brain barrier

J. Ruff[a], S. Hüwel[b], Marcelo J. Kogan[c,d], Ulrich Simon[a,*], Hans-Joachim Galla[b,*]

[a]*Institute of Inorganic Chemistry, RWTH Aachen University, Aachen, Germany*
[b]*Institute of Biochemistry, University of Münster, Münster, Germany*
[c]*Laboratorio de Nanobiotecnología, Facultad de Ciencias Químicas y Farmacéuticas, Universidad de Chile, Santiago de Chile, Chile*
[d]*Advanced Center for Chronic Diseases (ACCDiS), Santiago de Chile, Chile*

Received 24 October 2016; accepted 24 February 2017

**Abstract**

We studied the effect of gold nanoparticle (AuNP) size, surface charge, concentration and morphology on the integrity of the blood–brain barrier (BBB) in a well-established *in vitro* model set-up. We focused on the effect of peptide functionalized hollow gold nanospheres and gold nanorods, which selectively bind to amyloidogenic β-amyloid structures. These AuNP conjugates have already been successfully tested as photothermal absorbers for potential application in Alzheimer's disease (AD) therapy in an *in vitro* set-up, but may exhibit a low passage through the BBB due to their overall negative charge. Our results show that: (i) small (1.4 nm) AuNPs strongly affects the BBB integrity, (ii) negative surface charge impedes BBB passage, and (iii) this charge effect caused by the peptide is compensated by covalent coupling to a polyethylene glycol ligand stabilizing the particles in diluted manner.


*Key words:* Hollow gold nanospheres; Gold nanorods; Blood–brain barrier; Impedance spectroscopy

Neurodegenerative diseases have become a major health problem worldwide.[1–3] The development of approaches that can cure diseases or that can prolong the lifetime of affected people, is therefore of particular interest.[1,2] However, intravenously administered treatments are limited by the accessibility of the drugs to the brain because they have to overcome among others the blood–brain barrier (BBB) prior to reaching the target. The BBB is one of the main entrances to the central nervous system. The barrier is located within the cerebral capillaries at the interface between the blood circulation and cerebral tissue and consists mainly of capillary endothelial cells that are closely connected by tight junctions preventing uncontrolled paracellular flux.[4–6] Since the transport across the BBB represents the rate-determining step of drug delivery into the brain, the development of most central nervous system drugs is halted before completion due to their poor brain permeability.[7] The characterization of BBB permeability by *in vitro* models is therefore crucial and required as early as possible during drug development. Nowadays, a variety of well-established *in vitro* tests based on cultured cell models exists.[8] One well established *in vitro* model set-up, mimicking both the barrier and carrier functions of the BBB expressed *in vivo*, is based on the measurement of the transendothelial electric resistance (TER) and the capacity ($C_{CL}$) of a porcine brain capillary endothelial (PBCE) cell layer cultured on membrane by impedance spectroscopy.[6,9–13]

Plasmonic gold nanoparticles (AuNP) may be of potential use for diagnostics and therapy of neurodegenerative diseases is a very promising approach. AuNPs display localized surface plasmon resonance (LSPR),[14,15] a property that is unique to the nanostructured form and is absent in the bulk metal. The LSPR makes the particle absorb and scatter light very efficiently at certain wavelengths and parts of the absorbed light are dissipated locally as heat known as the photothermal effect. In this way the same nanomaterial can be used for diagnostics or therapy and for the so-called nanotheranostics, which represents a combination

J.R. and U.S. are grateful for financial support from the Excellence Initiative of the German federal and state Governments (I[3]TM Seed Fund). M.J.K. gratefully acknowledges financial support from Fondap 15130011 project.

*Corresponding authors.
*E-mail addresses:* ulrich.simon@ac.rwth-aachen.de (U. Simon), gallah@uni-muenster.de (H.-J. Galla).

http://dx.doi.org/10.1016/j.nano.2017.02.013
1549-9634/

of both.[16] For biomedical purposes, it is important to consider the high absorbance of biological tissue caused by water, hemoglobin and lipids. Biological tissue provides a so-called "spectral window" located in the near infrared (NIR) range where its auto-absorption is reduced to a minimum. In this region, the highest penetration depth of light and the highest contrast with regard to tissue can be achieved.[17] By controlling AuNP size and morphology, the spectral position of the wavelengths of maximum absorbance can be adjusted to this range.[18] NIR-absorbing hollow gold nanospheres (HAuNS) and gold nanorods (AuNR) were therefore designed to tackle this issue.[19,20] A further benefit of AuNP is their ability to absorb light of a certain wavelength and to transform it into heat, which is then delivered to the nearby surroundings of the particles.[18,20–22] The thermal energy can thus be applied for therapeutic purposes, in particular in photothermal therapy (PTT) of neurodegenerative diseases such as Alzheimer's disease (AD).[23–26] The latter context, where the formation of Aβ fibrils starting from amyloidogenic Aβ structures is reported as one reason for AD, is of particular importance to develop new methodologies that would allow an early detection and disaggregation of toxic Aβ aggregates.[27]

The disaggregation of Aβ toxic aggregates could be achieved by using AuNP equipped with peptides such as the CLPFFD peptide which selectively binds to the hydrophobic domains of amyloidogenic A*β* structures. CLPFFD bears a cysteine group at the N-terminus and thus can be covalently bound to gold surface *via* an SH moiety, so that the AuNP can selectively bind the amyloidogenic structures. The sequence LPFFD is a fragment corresponding to the physiological molecule Aβ(1-42) and recognizes a particular (hydrophobic) domain of the β-sheet structure (the sequence $^{17}$LVF$^{20}$F which is one of the hydrophobic cores of the native protein Aβ. In previous work we demonstrated that the position of the hydrophobic residues L, F and F is critical to achieve the selectivity for the binding of the peptide AuNP to the amyloidogenic structures.[28]

Recently, we demonstrated the suitability in disaggregation of Aß *in vitro* by using HAuNS and AuNR functionalized with those CLPFFD-peptides in two different ways.[29] The peptide was either directly bound to the particle surface by covalent binding with its SH moiety to the AuNP surface or indirectly by binding the peptide covalently to a particle-protecting polyethylene glycol (PEG) ligand shell. For the indirect functionalization, the peptides are covalently coupled to $H_2N$-terminated thiol-PEG ligands, respectively, which in turn are embedded into a thiol-PEG-$OCH_3$ ligand shell. The presence of the PEG ligands in addition to the peptide on the AuNP surface favors not only the biocompatibility of the particles but also the interaction with Aβ structures since PEG ligands themselves favor this interaction and can even influence the aggregation of Aβ.[30–32] However, this interaction is not selective and it thus cannot be ruled out that the PEG interacts with other proteins in the biological system. These results prompted the question whether these particles are able to cross the BBB in a way that a therapeutically needed amount of nanoparticles crosses the barrier without affecting its integrity and the accurate function of the brain. Therefore, we carried out in this work basic *in vitro* BBB crossing studies in the well established *in vitro* model set-up based on the measurement of the transendothelial electric resistance (TER) and the capacity ($C_{CL}$) of a porcine brain capillary endothelial (PBCE) cell layer cultured on membrane by impedance spectroscopy. The aim of our performed study was to evaluate the effect on the BBB integrity and the BBB permeability of four different parameters: the effect of AuNP size, AuNP surface charge and functionality, AuNP concentration and AuNP morphology.

## Materials and methods

### *Nanoparticle preparation and characterization*

In the following, AuNPs are denoted by considering their geometry: AuNS = Au nanospheres, AuNR = Au nanorods and HAuNS = hollow Au nanospheres. 1.4 nm AuNS functionalized with negatively-charged monosulfonated triphenylphosphine (TPPMS) ligands (AuNS1.4-MS) and 15 nm AuNS functionalized with TPPMS ligands (AuNS-MS) were synthesized as described previously.[33,34]

15 nm AuNS functionalized with neutral methoxy terminated polyethylene glycol (mPEG) ligands (AuNS-mPEG) were prepared by a ligand exchange reaction starting from citrate stabilized 15 nm AuNS (AuNS-Cit), which are themselves obtained following the well-known Turkevich method.[35] HAuNS functionalized with mPEG ligands (HAuNS-mPEG) or directly (HAuNS-CLPFFD) and indirectly with CLPFFD-peptides (HAuNS-mPEG-CLPFFD) were obtained by a ligand exchange reaction starting from HAuNS-Cit, synthesized as described previously *via* a sacrificial galvanic replacement reaction starting from cobalt nanoparticles.[36,37] AuNR functionalized with mPEG ligands (AuNR-mPEG) or directly (AuNR-CLPFFD) and indirectly with CLPFFD-peptides (AuNR-mPEG-CLPFFD) were prepared by a ligand exchange reaction starting from cetyltrimethylammonium bromide (CTAB) stabilized AuNR (AuNR-CTAB) synthesized as described previously *via* a seed-mediated growth reaction.[29,37] The ligand exchange reaction leading to AuNR-mPEG is in analogy to HAuNS-mPEG preparation and has been described in detail previously.[37] AuNR-CLPFFD were synthesized as described previously.[26] HAuNS-CLPFFD were obtained in a homogeneous ligand exchange reaction starting from the crude HAuNS-Cit with a larger ligand excess. AuNR-mPEG-CLPFFD are as well obtained in analogy to HAuNS-mPEG-CLPFFD preparation and the synthesis is descried in detail in our previous paper.[29] For this indirect functionalization of HAuNS and AuNR with CLPFFD-peptides, particles with a mixed PEG ligand shell composed of mPEG (95%) and amino terminated mPEG ligands ($PEG\text{-}NH_2$), to which the peptide is bound covalently *via* an SMCC coupling chemistry, were prepared. Those particles, denoted as HAuNS-mPEG-$NH_2$ and AuNR-mPEG-$NH_2$ were listed here only as intermediate state in order to show the successful peptide functionalization of the particles. The dimensions of the prepared AuNP were obtained either by transmission electron microscopy (TEM) in the case of the AuNS1.4MS or for the larger particles by scanning electron miscropscopy in transmission mode (SEM-T) measurements. Moreover, the conjugates were characterized by optical extinction spectroscopy (OES), dynamic light scattering (DLS)

Table 1
Optical extinction and ligand composition of the investigated AuNP.

| | Dimensions [nm] | dH [nm] | Absorbance maximum [nm] | Zeta-potential [mV] |
|---|---|---|---|---|
| AuNS1.4-MS | $d$ = 1.4 ± 0.2 | / | / | / |
| AuNS-MS | $d$ = 14.3 ± 1.1 | / | 524 | −64 |
| AuNS-Cit | $d$ = 14.8 ± 1.5 | 23 | 519 | −42 |
| AuNS-mPEG | $d$ = 14.8 ± 1.5 | 42 | 521 | −13 |
| HAuNS-Cit | $d_{outer}$ = 38.0 ± 8.1<br>$d_{inner}$ = 27.9 ± 7.0 | 52 | 885 | −42 |
| HAuNS-mPEG | $d_{outer}$ = 37.1 ± 7.7<br>$d_{inner}$ = 27.2 ± 7.0 | 66 | 849 | −0.3 |
| HAuNS-mPEG-$NH_2$ | / | 67 | 828 | +0.1 |
| HAuNS-mPEG-CLPFFD | $d_{outer}$ = 35.8 ± 9.0 $d_{inner}$ = 26.8 ± 8.8 | 67 | 825 | −16 |
| HAuNS-Cit (batch 2) | $d_{outer}$ = 45.0 ± 9.8 $d_{inner}$ = 36.8 ± 8.9 | 61 | 889 | −47 |
| HAuNS-CLPFFD | $d_{outer}$ = 44.8 ± 9.4<br>$d_{inner}$ = 32.0 ± 9.2 | 65 | 855 | −67 |
| AuNR-CTAB | $l$ = 57.2 ± 8.0<br>$w$ = 14.3 ± 3.0 | 96 | 510/805 | + 33 |
| AuNR-mPEG | $l$ = 60.2 ± 8.0<br>$w$ = 15.3 ± 3.1 | 120 | 510/814 | −2 |
| AuNR-CLPFFD | $l$ = 43.3 ± 8.0<br>$w$ = 11.7 ± 2.3 | / | 515/732 | +56 |
| AuNR-mPEG-$NH_2$ | / | 114 | 511/812 | −16 |
| AuNR-mPEG-CLPFFD | $l$ = 60.1 ± 9.0<br>$w$ = 13.7 ± 2.5 | 100 | 510/815 | −26 |

Regarding the dimension, for AuNS the outer diameter, for AuNR the length and width and for HAuNS the outer and inner diameter as well as the respective standard deviations in all cases are given together with the hydrodynamic diameter dH and the zeta-potential. Regarding the optical extinction, for AuNS and AuNR the absorbance maximum and for AuNR the longitudinal and transversal absorbance maximum are given.

and zeta potential measurements (ξ-pot) in order to prove the successful ligand exchange reaction. More detailed information on the nanoparticle preparation and characterization methods is reported in the supplementary material. The obtained values are shown and discussed in the Results section.

### *Transcellular electrical resistance measurements and permeability measurements*

Endothelial cells form tight junctions, which minimize the paracellular diffusion and act like an ohmic resistor increasing the TER, the transendothelial or transepithelial electrical resistance. Therefore, the TER measurement is a reliable tool to analyze the integrity and tightness of a cellular monolayer. During transfer studies, the integrity of the BBB model was monitored using a cellular impedance spectrometer, the CellZscope device from Nanoanalytics (Münster, Germany). In impedance spectroscopy the frequency of an applied AC voltage is swept while measuring the amplitude and the phase of the resulting AC, the transendothelial or transepithelial electrical resistance current. The resulting total impedance, $Z$, contains information not only about the TER, but also the capacitance ($C_{CL}$) of the cell layer can be extracted and provided as a readout parameter for the integrity of the cell layer. This non-invasive method can be applied to living cells without markers and allows them to be monitored during growth and differentiation. Details are given elsewhere.[11,13]

Prior to the measurements, PBCE cells were seeded on rat tail collagen coated (Matrigel™-coated) microporous polycarbonate membrane filters (Corning, Wiesbaden, Germany, 0.4 μm pores; 1.13 $cm^2$ growth area) and cultured as describe by Cramer et al.[6] Only PBCE cells with capacitance between 0.45 μF/$cm^2$ and 0.6 μF/$cm^2$, revealing a confluent cell monolayer and resistance higher 500 Ω/$cm^2$ were used. AuNPs at different NP concentrations were added to the filters and the TER and $C_{CL}$ of the cells were monitored in a triplicate during 24 h with the *CellZscope* device. The obtained TER values were normalized to their corresponding starting TER in the absence of AuNP. To investigate the permeability of the AuNP through the BBB, the medium from the apical and the basolateral side was collected and analyzed regarding the respective gold content by atomic absorption spectrometry (AAS). The passage of the AuNP through the BBB after 24 h, expressed in %, is obtained from the ration between the initial NP concentration and the determined basolateral NP concentration.

## Results

In order to explore the effect of AuNP size, AuNP surface charge, AuNP concentration and AuNP morphology on the BBB integrity, differently functionalized AuNPs have been prepared. AuNS1.4MS and AuNS-MS were prepared in accordance to literature protocols.[29,34,37] For further details see the supplementary material. HAuNS-mPEG, HAuNS-CLPFFD and HAuNS-mPEG-CLPFF of about 40 nm in diameter and AuNR-mPEG, AuNR-CLPFFD and AuNR-mPEG-CLPFFD with 60 nm length and 15 nm width, were synthesized according to procedures previously described.[29,37,38] Dimensions, zeta-potential and corresponding optical extinction properties of the samples are summarized in Table 1, whereas the corresponding figures and images are shown in the supplementary material. For larger particles the absorbance is dominated by the surface plasmon resonance. For particles smaller than 2 nm, a broad band absorption extending across the whole visible region from about 250 nm to 1350 nm is observed. Therefore, no surface

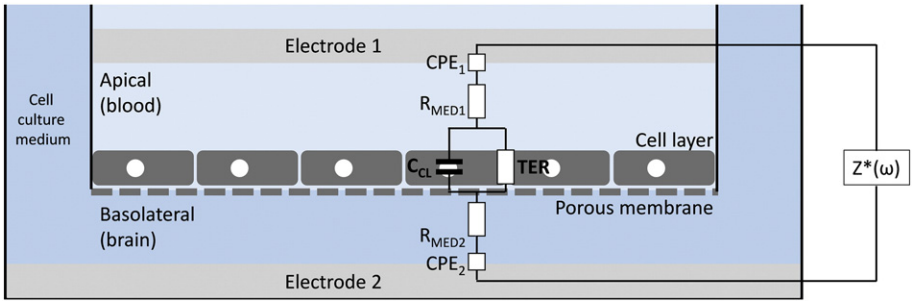


Figure 1. Schematic illustration of an *in vitro* BBB model and the electric circuit applied to analyze the data. Endothelial PBCE cells are grown on a permeable filter forming an interface mimicking the basolateral (brain) and apical (blood) side *in vivo*. The layer properties are characterized by the transepithelial electric resistance (TER) and the capacity ($C_{CL}$) by measuring the frequency-dependent total impedance ($Z^*(\omega)$) of the system. The cell culture medium in both compartments is modeled by simple ohmic resistance ($R_{MED}$) and the interface between the electrodes and the cell culture medium is described by a constant phase element (CPE). The electric equivalent circuit is developed to analyze the data and to separate the impedance contribution from the cells from the rest of the system. The figure is not drawn to scale.

plasmon resonance absorbance maximum is given in the case of the AuNS1.4-MS.

The influence of AuNS on the BBB integrity was evaluated with the well established *in vitro* model set-up[11–13] by measuring the TER and the $C_{CL}$ of a PBCE cell layer cultured on membranes during 24 h. In Figure 1 the used model set-up as well as the electric circuit applied to analyze the data is schematically drawn according to that reported.[11–13]

In this *in vitro* model set-up the recorded total impedance ($Z^*(\omega)$) includes the TER and the $C_{CL}$. Additionally, the cell culture medium and the interface between the medium and the electrodes contribute as well to $Z^*(\omega)$. The TER establishes a direct correlation between the permeability of a cell layer and its electric resistance. From the capacity information about the cell layer properties itself are gained. Thereby tight cell layers exhibit high electric resistance and vital cell low capacities. By modeling the system by basic elements, i.e., the cell culture medium by a simple ohmic resistance ($R_{MED}$) and the interface between the electrodes and the cell culture medium by a constant phase element (CPE), a simple non-linear frequency dependency of the total impedance of the system was found. By fitting the experimental data by an algorithm function, the TER and $C_{CL}$ of living cell were obtained.[11–13] In principle a decreased TER indicates a breakup of the barrier properties whereas an increase of the $C_{CL}$ arises from a change in the cell morphology or the removal of the cells from the membrane up to the cell death. The amount of AuNP passed through the barrier is expressed in percentage and evaluated by the ratio between the initially applied gold concentration and the basolateral gold concentration determined by AAS.

### *Effect of TPPMS, mPEG and CLPFFD ligands on the BBB integrity and the PBCE cells*

First, the influence on the integrity of the BBB and the PBCE cells of the pure ligands stabilizing the AuNP was investigated in the *in vitro* model set-up. Therefore, PBCE cells were incubated in the presence of two different ligand concentrations. First was with 3.3 μM TPPMS, 400 μM mPEG or 25 μM CLPFFD-peptide, respectively, corresponding to the concentration range in which the ligands are present on the AuNP surface. Additionally, in order to evaluate the effect of higher ligand concentration, the PBCE cells were incubated with the 10-fold concentration of TPPMS, mPEG and CLPFFD, respectively. In

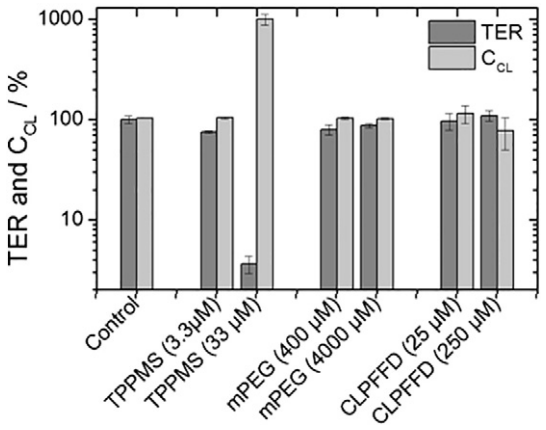


Figure 2. The influence of the ligands TPPMS, mPEG and CLPFFD on PBCE cells and BBB integrity. TER and $C_{CL}$ values after treatment of PBCE cell monolayers with TPPMS, mPEG or CLPFFD applied at a respective concentration of 3.3 μM, 400 μM or 25 μM and 33 μM, 4000 μM or 250 μM. The values are expressed relative to their respective starting value prior to NP addition and as means, $n = 3$. The absolute TER ranged between 250 $\Omega \cdot cm^2$ and 500 $\Omega \cdot cm^2$. The ordinate is given in a logarithmic scale for a better overview.

Figure 2 the mean TER and the $C_{CL}$ after 24 h (time needed for re-equilibration; *cf.* Ref. 12) regarding the respective starting values prior to ligand addition from $n = 3$ experiments are shown. All recorded values for the TER and the $C_{CL}$ during the 24 h are displayed in the supplementary material.

The TER and the $C_{CL}$ values recorded after 24 h show that TPPMS induces a concentration-dependent strong decrease of the TER from 100% to 3.6% and an increase of the $C_{CL}$ by factor 10. This indicates that TPPMS at a concentration of 33 μM influences the BBB integrity and initiates cell death. In contrast, mPEG and CLPFFD show at both investigated concentrations no significant influence on the BBB integrity and the cell morphology.

### *Effect of AuNP size and surface charge on the BBB integrity and the PBCE cells*

AuNS1.4-MS (1.4 nm) and AuNS-MS (15 nm) were applied at the equal gold concentration of 75 mg Au/L in the *in vitro* set-up. These two particle species are expected to follow a

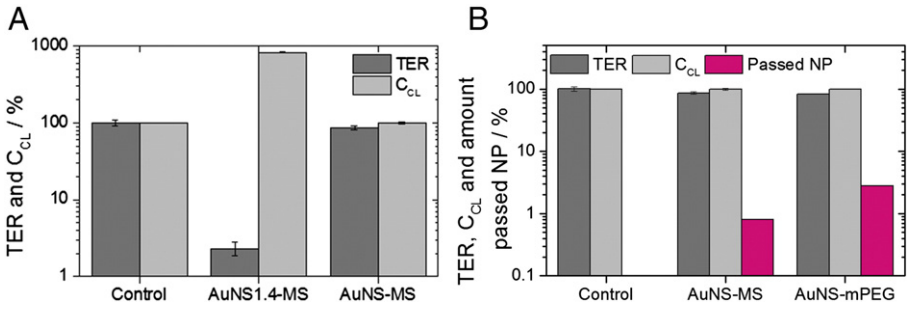


Figure 3. The influence of AuNP size and surface charge on PBCE cells and BBB integrity. TER and $C_{CL}$ values after treatment of PBCE cell monolayers with (**A**) AuNS1.4-MS and AuNS-MS at the same gold concentration of 75 mg Au/L and (**B**) AuNS-MS and AuNS-mPEG at the same NP concentration of 0.36 nM. The values are expressed relative to their respective starting value prior to NP addition and as means, $n = 3$. The absolute TER ranged between 250 $\Omega \cdot cm^2$ and 500 $\Omega \cdot cm^2$. The ordinate is given in a logarithmic scale for a better overview.

different pathway during BBB passing, due to size-effects: the small AuNS1.4MS might be able to cross the BBB by a paracellular pathway through the tight junctions, whereas the AuNS-MS are supposed to follow a transcellular pathway mediated by endocytosis of the NP. The effect of the AuNP surface charge on the BBB integrity and the PBCE cells was investigated by applying negatively charged AuNS-MS (15 nm) and neutrally charged AuNS-mPEG (15 nm) at the same NP concentration of 0.36 nM in the *in vitro* set-up. In Figure 3 the overview of the recorded mean from $n = 3$ experiments TER and $C_{CL}$ values after 24 h regarding the respective starting values prior to NP addition as well as the amount of passed AuNP through the barrier is shown. The corresponding recorded TER and $C_{CL}$ curves during 24 h are displayed in the supplementary material.

As shown in Figure 3, *A*, the AuNS1.4-MS induce a decrease of the TER from 100% to 2.3% and an increase of the $C_{CL}$ by a factor of 8. AuNS-MS display no change in the TER and $C_{CL}$ values compared to the control sample. This indicates that the AuNS1.4-MS affect the BBB integrity and provoke cell death, whereas the AuNS-MS have no influence on the BBB integrity at the investigated concentration. The pronounced effect of AuNS1.4-MS on the BBB integrity is in agreement with the high toxicity reported for these particles.[32,39] In the case of AuNS1.4-MS no amount of passed AuNP through the BBB was determined. The collapse of the tight junctions and correlated break-up of the membrane allows the NP to pass unhindered through the membrane.

Figure 3, *B* shows the effect of surface charge on the BBB integrity. For the two investigated particles, namely AuNS-MS (15 nm) and AuNS-mPEG (15 nm), the TER and $C_{CL}$ values are equal with the control sample for both investigated particle species. This indicates that neither the AuNS-MS nor the AuNS-mPEG showed an influence on the BBB integrity or the PBCE cells at the investigated NP concentration. As shown in Figure 3, *B*, the AuNS-mPEG provides with 2.8% a higher amount of passed NP through the BBB compared to the AuNS-MS with 0.8%. The TER remaining at high values around 100% relates to closed tight junctions, indicating a transcellular pathway by endocytosis of both NP species.[40] In general, positively-charged particles have been demonstrated to more effectively pass the BBB compared to neutral and negatively-charged ones.[12] The negatively-charged particles are even repelled from the negatively-charged cell membrane due to electrostatic repulsion. The protein corona formation allowing faster cell internalization is higher for charged particles than for neutral PEGylated particles. This leads to a high cellular uptake of the negatively-charged AuNS-MS which is in accordance to literature.[41] However, the electrostatically-stabilized AuNPs experience only a low stability in biological medium and consequently aggregate very fast in the *in vitro* model set-up compared to the PEGylated particles because the set-up is filled with cell culture medium. This could be observed visually for AuNS-MS by the formation of a black precipitate in the filter after the 24 h incubation time. This shows that small (1.4 nm) AuNPs strongly affect the BBB integrity, while for larger ones (15 nm and above), which are stabilized by negatively charged MS, show limited stability in cell culture media and the negative surface charge impedes BBB passage, both being in contrast to PEGylated particles.

### *Effect of AuNP concentration on the BBB integrity and the PBCE cells*

AuNS-mPEG (15 nm) particles showed highest stability in the *in vitro* model set-up. Therefore, these particles were taken in order to explore the effect of the AuNP concentration on the BBB integrity and NP passing through the BBB, as a proof of concept. One might assume that equilibrium between the upper and lower filter compartment is aimed at with increasing incubation time. Therefore, a higher amount of NP going through the barrier is expected at higher NP concentration.

AuNS-mPEG (15 nm) at a NP concentration of 0.14 nM, 0.36 nM, 4.2 nM and 8.5 nM were applied in the *in vitro* set-up. In Figure 4 the mean TER and the $C_{CL}$ after 24 h from $n = 3$ experiments regarding the respective starting values prior to NP addition as well the amount of AuNS passed through the barrier are shown. All recorded values for the TER and the $C_{CL}$ during the 24 h are displayed in the supplementary material.

In Figure 4 no significant decrease of the TER and the $C_{CL}$ values after 24 h compared to the control samples is observable at any concentration. This indicates that the particles show no significant influence on the BBB integrity at the investigated AuNS concentrations. The highest amount of AuNS passed through the BBB with 2.8% is reached at a concentration of 0.36 nM followed by an amount of 0.08% at 0.14 nM, 0.5% at 4.2 nM and 0.6% at a NP concentration of 8.5 nM.

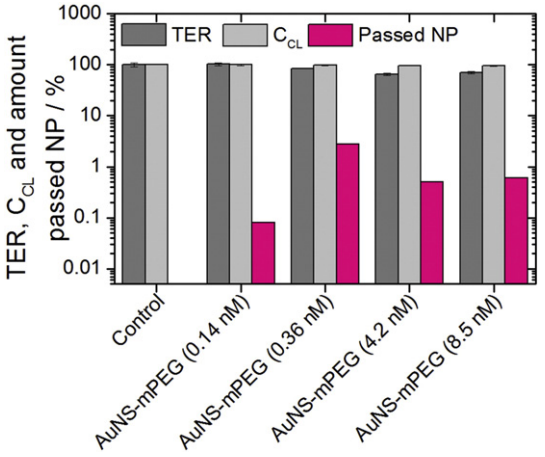


Figure 4. The influence of AuNP concentration on PBCE cells and BBB integrity. TER and $C_{CL}$ values after treatment of PBCE cell monolayers with AuNS-MPEG at the NP concentrations of 0.14 nM, 0.36 nM, 4.2 nM and 8.5 nM. The values are expressed relative to their respective starting value prior to NP addition and as means, $n = 3$. The absolute TER ranged between 250 $\Omega \cdot cm^2$ and 500 $\Omega \cdot cm^2$. The ordinate is given in a logarithmic scale for a better overview.

With increasing concentration of applied AuNS from 0.14 nM to 0.36 nM the amount of passed AuNS first increases from 0.08% to 2.8%. However, by further increasing the AuNS concentration, the detected amount of passed AuNS through the BBB decreases, which represents an unexpected finding. Previously reported studies on the crossing potential of silica NP through the BBB reported enhanced silica NP entrance upon high silica NP concentration (1 mg/mL). The authors of this study ascribed the high transport at high particle concentration to a damage of the tight junction resulting in a break-up of the barrier properties.[42] In our studies, the tight junction and the cells are still intact because no increase in the capacity is recorded. We assume that the low amount of passed NP through the BBB at high AuNS concentrations (4.2 nM and 8.5 nM) is related to a saturation of the cell monolayer with the AuNS lowering further uptake.

### *Effect of AuNP morphology and peptide coupling on the BBB integrity and the PBCE cells*

NIR-absorbing AuNPs are promising candidates in nanomedicine. NIR-absorbing AuNPs are obtained by changing the AuNP morphology to HAuNS or AuNR. Therefore, we compared AuNS, HAuNS and AuNR with same surface functionalization, which are mPEG ligands, in the *in vitro* model set-up. AuNS-mPEG, HAuNS-mPEG and AuNR-mPEG were applied in the *in vitro* model set-up at the equal NP concentration of 0.14 nM. In Figure 5 the overview of the recorded mean TER, the $C_{CL}$ from $n = 3$ experiments with respect to the corresponding starting values prior to NP addition and the amount of NP passed through the BBB after 24 h is given. All recorded values for the TER and the $C_{CL}$ during the 24 h are displayed in the supplementary material.

The AuNS-mPEG, HAuNS-mPEG and AuNR-mPEG show constant TER and $C_{CL}$ values of 100% after 24 h. The constant TER and $C_{CL}$ values indicate that different AuNP morphologies have no influence on the BBB integrity and the PBCE cells. The highest amount of AuNP passed through the BBB is obtained for AuNS-mPEG with 0.08% followed by the AuNR-mPEG with 0.02% and the HAuNS-mPEG with 0.01%. This behavior is in accordance to literature findings, reporting high BBB transport of 18 nm AuNS.[41] HAuNS-mPEG of 43 nm in diameter showed a similar low BBB permeability *in vivo* as well.[43]

The overall very low amount of AuNP passed into the brain can be explained by the previously discussed concentration-dependent BBB permeability.[41] According to the reported suitability in AD therapy of HAuNS and AuNR directly or indirectly functionalized with CLPFFD-peptides[29] a main part of the here reported study focuses on the ability of these particles to cross the BBB in a way that a therapeutically needed amount of nanoparticles crosses the barrier without affecting its integrity and the accurate function of the brain. HAuNS-CLPFFD, HAuNS-mPEG-CLPFFD, AuNR-CLPFFD and AuNR-mPEG-CLPFFD were applied in the *in vitro* model set-up at the equal NP concentration of 0.14 nM. This concentration was chosen to be suitable for a comparison with the *Aβ*-fibrillation study previously reported in the literature.[24] In Figure 5 the overview of the recorded mean TER, the $C_{CL}$ from $n = 3$ experiments with respect to the corresponding starting values prior to NP addition and the amount of NP passed through the BBB after 24 h is given. All recorded values for the TER and the $C_{CL}$ during the 24 h are displayed in the supplementary material.

First looking at the directly functionalized particles: HAuNS-CLPFFD show a decrease of the TER to 52% but no increase of the $C_{CL}$ value and AuNR-CLPFFD show a strong decrease of the TER to 3% and a pronounced increase of the $C_{CL}$ value. The collapse of the BBB and induced cell death can be attributed to the high toxicity of these particles. Especially, the AuNR-CLPFFD have a high cytotoxicity in HeLa cells and SH-SY5Y cells originating from remaining CTAB molecules after functionalization.[26,29,37] The amount of HAuNS-CLPFFD passing the BBB is only half of the amount for HAuNS-mPEG which is in accordance to the heretofore shown results for AuNS-MS and AuNS-mPEG. For the AuNR-CLPFFD no amount of passed NP was determined, reflecting the complete collapse of the barrier.

Second looking at the indirectly functionalized particles, we found that when the CLPFFD-peptides are coupled in a diluted manner to the PEG ligand shell as in the case of HAuNS-mPEG-CLPFFD and AuNR-mPEG-CLPFFD, no difference in the BBB integrity, cell morphology or passage rate compared to the fully mPEG functionalized HAuNS-mPEG and AuNR-mPEG particles, respectively, is noticeable.

Overall the amount of nanoparticles passing the BBB at the dose applied in our studies is very low and far from being enough for an application in the brain. For applications in clinical settings, the passage of the conjugates must be significantly enhanced. This can be reached for example by longer circulations times *in vivo* or a peptide which causes the active transport of the AuNP conjugates through the BBB.[25]

## Discussion

Our experimental results demonstrate that the integrity of the BBB is strongly affected by small (1.4 nm) AuNP; they affect the

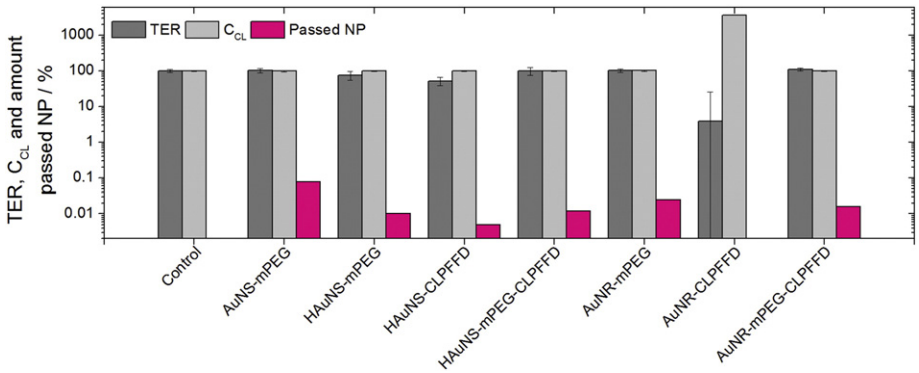


Figure 5. The influence of differently functionalized HAuNS and AuNR on PBCE cells and BBB integrity. TER and $C_{CL}$ values after treatment of PBCE cell monolayers with AuNS-mPEG, HAuNS-mPEG, HAuNS-CLPFFD or HAuNS-mPEG-CLPFFD as well as AuNR-mPEG, AuNR-CLPFFD or AuNR-mPEG-CLPFFD at a NP concentration of 0.14 nM. The values are expressed relative to their respective starting value prior to NP addition and as means, $n = 3$. The absolute TER ranged between 250 $\Omega \cdot cm^2$ and 500 $\Omega \cdot cm^2$. The ordinate is given in a logarithmic scale for a better overview.

BBB integrity and provoke cell death. This pronounced effect of AuNS1.4-MS is in agreement with the high toxicity reported for these particles before. For all larger particles, negative surface charge impedes BBB passage mainly caused by the negative surface charge of the cells. However, this impeding effect can be compensated in the specific case of negatively charged peptides selectively binding to amyloidogenic β-amyloid structures, when the peptide is covalently coupled to a PEG ligand stabilizing the particles in diluted manner. This is, regarding the huge potential of these NIR-absorbing AuNP in nanomedicine, especially in AD therapy, of high relevance. In future studies, the functionalization of HAuNS and AuNR with peptides in order to increase the BBB permeability and the NP concentration in the brain is of particular interest. Thereby, multivalent peptides which selectively bind to A*β*-amyloid fibrils and cause the active transport of the AuNP conjugates through the BBB are most promising. Furthermore, *in vivo* studies have to be conducted.

## Appendix A. Supplementary data

Supplementary data to this article can be found online at http://dx.doi.org/10.1016/j.nano.2017.02.013.

## References


1. Petersen RC, Caracciolo B, Brayne C, Gauthier S, Jelic V, Fratiglioni L. Mild cognitive impairment: a concept in evolution. *J Intern Med* 2014;**275**:214-28.
2. Prince M, Bryce R, Albanese E, Wimo A, Ribeiro W, Ferri CP. The global prevalence of dementia: a systematic review and metaanalysis. *Alzheimers Dement* 2013;**9**(1):63-75.
3. Wimo A, Winblad B, Aguero-Torres H, von Strauss E. The magnitude of dementia occurrence in the world. *Alzheimer Dis Assoc Disord* 2003;**17**(2):63-7.
4. Ballabh P, Braun A, Nedergaard M. The blood–brain barrier: an overview: structure, regulation, and clinical implications. *Neurobiol Dis* 2004;**16**(1):1-13.
5. Weiss N, Miller F, Cazaubon S, Couraud P-O. The blood–brain barrier in brain homeostasis and neurological diseases. *Biochim Biophys Acta* 2009;**1788**(4):842-57.
6. Cramer S, Tacke S, Bornhorst J, Sachan AK, Klingauf J, Schwerdtle T, et al. The influence of silver nanoparticles on the blood–brain and the blood–cerebrospinal fluid barrier in vitro. *J Nanomed Nanotechnol* 2014;**5**(5):1-12.
7. Ke W, Shao K, Huang R, Han L, Liu Y, Li J, et al. Gene delivery targeted to the brain using an Angiopep-conjugated polyethyleneglycol-modified polyamidoamine dendrimer. *Biomaterials* 2009;**30**(36):6976-85.
8. Helms HC, Abbott NJ, Burek M, Cecchello R, Couraud P-O, Deli MA, et al. In vitro models of the blood–brain barrier: an overview of commonly used brain endothelial cell culture models and guidelines for their use. *J Cereb Blood Flow Metab* 2016;**0**:1-29.
9. Lohmann C, Hüwel S, Galla HJ. Predicting blood–brain barrier permeability of drugs: evaluation of different in vitro assays. *J Drug Target* 2002;**10**(4):263-76.
10. Prieto P, Blaauboer BJ, de Boer AG, Boveri M, Cecchelli R, Clemedson C, et al. Blood–brain barrier in vitro models and their application in toxicology. The report and recommendations of ECVAM. Workshop 49. *Altern Lab Anim* 2004;**32**(1):37-50.
11. Benson K, Cramer S, Galla H-J. Impedance-based cell monitoring: barrier properties and beyond. *Fluids Barriers CNS* 2013;**10**(5):1-11.
12. Qiao R, Gao M, Galla H-J. Nanoparticles: important tools to overcome the blood–brain barrier and their use for brain imaging. In: Chen X, Fuchs H, editors. *Soft Matter Nanotechnology*. Wiley-VCH Verlag GmbH & Co. KGaA; 2015. p. 109-30.
13. cellZscope®—the automated cell monitoring system. Available from: http://www.nanoanalytics.com/en/hardwareproducts/cellzscope/.
14. Kelly KL, Coronado E, Zhao LL, Schatz GC. The optical properties of metal nanoparticles: the influence of size, shape, and dielectric environment. *J Phys Chem B* 2003;**107**(3):668-77.
15. Huang X, El-Sayed MA. The optical properties of metal nanoparticles: the influence of size, shape, and dielectric environment. *J Adv Res* 2010;**1**(1):13-28.
16. Sharma H, Mishra PK, Talegaonkar S, Vaidya B. Metal nanoparticles: a theranostic nanotool against cancer. *Drug Discov Today* 2015;**20**(9):1143-51.
17. Bashkatov AN, Genina EA, Kochubey VI, Tuchin VV. Optical properties of human skin, subcutaneous and mucous tissues in the wavelength range from 400 to 2000 nm. *J Phys Appl Phys* 2005;**38**(15):2543-55.
18. Lal S, Link S, Halas NJ. Nano-optics from sensing to waveguiding. *Nat Photon* 2007;**1**(11):641-8.
19. Lu W, Xiong C, Zhang G, Huang Q, Zhang R, Zhang JZ, et al. Targeted photothermal ablation of murine melanomas with melanocyte-stimulating hormone analog-conjugated hollow gold nanospheres. *Clin Cancer Res* 2009;**15**(3):876-86.
20. von Maltzahn G, Park J-H, Agrawal A, Bandaru NK, Das SK, Sailor MJ, et al. Computationally guided photothermal tumor therapy using long-circulating gold nanorod antennas. *Cancer Res* 2009;**69**(9):3892-900.

21. Jain PK, Huang X, El-Sayed IH, El-Sayed MA. Noble metals on the Nanoscale: optical and photothermal properties and some applications in imaging, sensing, biology, and medicine. *Acc Chem Res* 2008;**41**(12):1578-86.
22. Melancon MP, Zhou M, Li C. Cancer theranostics with near-infrared light-activatable multimodal nanoparticles. *Acc Chem Res* 2011;**44**(10):947-56.
23. Cobley CM, Chen J, Cho EC, Wang LV, Xia Y. Gold nanostructures: a class of multifunctional materials for biomedical applications. *Chem Soc Rev* 2011;**40**(1):44-56.
24. Kogan MJ, Bastus NG, Amigo R, Grillo-Bosch B, Araya E, Turiel A, et al. Nanoparticle-mediated local and remote manipulation of protein aggregation. *Nano Lett* 2006;**6**(1):110-5.
25. Prades R, Guerrero S, Araya E, Molina C, Salas E, Zurita E, et al. Delivery of gold nanoparticles to the brain by conjugation with a peptide that recognizes the transferrin receptor. *Biomaterials* 2012;**33**(29):7194-205.
26. Adura C, Guerrero S, Salas E, Medel L, Riveros A, Mena J, et al. Stable conjugates of peptides with gold nanorods for biomedical applications with reduced effects on cell viability. *ACS Appl Mater Interfaces* 2013;**5**(10):4076-85.
27. Harrison JR, Owen MJ. Alzheimer's disease: the amyloid hypothesis on trial. *Br J Psychiatry* 2016;**208**(1):1-3.
28. Olmedo I, Araya E, Sanz F, Medina E, Arbiol J, Toledo P, et al. How changes in the sequence of the peptide CLPFFD-$NH_2$ can modify the conjugation and stability of gold nanoparticles and their affinity for β-amyloid fibrils. *Bioconjug Chem* 2008;**19**(6):1154-63.
29. Ruff J, Hassan N, Morales-Zavala F, Steitz J, Kogan MJ, Simon U. *CLPFFD-PEG functionalized NIR-ABSORBING HOLLOW GOLD NANOSPHERES AND GOLD NANORODS INHIBIT β-AMYLOID AGGREGATION*; 2017 [manuscript in preparation].
30. Brambilla D, Verpillot R, Le Droumaguet B, Nicolas J, Taverna M, Kóňa J, et al. PEGylated nanoparticles bind to and alter amyloid-beta peptide conformation: toward engineering of functional nanomedicines for Alzheimer's disease. *ACS Nano* 2012;**6**(7):5897-908.
31. Brambilla D, Verpillot R, Taverna M, De Kimpe L, Le Droumaguet B, Nicolas J, et al. New method based on capillary electrophoresis with laser-induced fluorescence detection (CE-LIF) to monitor interaction between nanoparticles and the amyloid-β peptide. *Anal Chem* 2010;**82**(24):10083-9.
32. Brambilla D, Verpillot R, De Kimpe L, Taverna M, Le Droumaguet B, Nicolas J, et al. Nanoparticles against Alzheimer's disease: PEG–PACA nanoparticles are able to link the aβ-peptide and influence its aggregation kinetic. *J Control Release* 2010;**148**(1):e112-3.
33. Pan Y, Neuss S, Leifert A, Fischler M, Wen F, Simon U, et al. Size-dependent cytotoxicity of gold nanoparticles. *Small* 2007;**3**(11):1941-9.
34. Schmid G, Pfeil R, Boese R, Bandermann F, Meyer S, Calis GH, et al. $Au_{55}[P(C_6H_5)_3]_{12}CI_6$—ein Goldcluster ungewöhnlicher Größe. *Chem Ber* 1981;**114**(11):3634-42.
35. Turkevich J, Stevenson PC, Hillier J. A study of the nucleation and growth processes in the synthesis of colloidal gold. *Discuss Faraday Soc* 1951;**11**(0):55-75.
36. Schwartzberg AM, Olson TY, Talley CE, Zhang JZ. Synthesis, characterization, and tunable optical properties of hollow gold nanospheres. *J Phys Chem B* 2006;**110**(40):19935-44.
37. Ruff J, Steitz J, Buchkremer A, Noyong M, Hartmann H, Besmehn A, et al. Multivalency of PEG-thiol ligands affects the stability of NIR-absorbing hollow gold nanospheres and gold nanorods. *J Mater Chem B* 2016;**4**(16):2828-41.
38. Gutrath BS, Beckmann MF, Buchkremer A, Eckert T, Timper J, Leifert A, et al. Size-dependent multispectral photoacoustic response of solid and hollow gold nanoparticles. *Nanotechnology* 2012;**23**(22):225707.
39. Broda J, Küster A, Westhues S, Fahrenkamp D, Vogg ATJ, Steitz J, et al. Assessing the intracellular integrity of phosphine-stabilized ultrasmall cytotoxic gold nanoparticles enabled by fluorescence labeling. *Adv Healthc Mater* 2016;**5**:3118-28.
40. Wagner S, Kufleitner J, Zensi A, Dadparvar M, Wien S, Bungert J, et al. Nanoparticulate transport of oximes over an in vitro blood–brain barrier model. *PLoS One* 2010;**5**(12):e14213.
41. Leifert A, Pan-Bartnek Y, Simon U, Jahnen-Dechent W. Molecularly stabilised ultrasmall gold nanoparticles: synthesis, characterization and bioactivity. *Nanoscale* 2013;**5**(14):6224-42.
42. Hanada S, Fujioka K, Inoue Y, Kanaya F, Manome Y, Yamamoto K. Cell-based in vitro blood–brain barrier model can rapidly evaluate nanoparticles' brain permeability in association with particle size and surface modification. *Int J Mol Sci* 2014;**15**(2):1812-25.
43. You J, Zhou J, Zhou M, Liu Y, Robertson JD, Liang D, et al. Pharmacokinetics, clearance, and biosafety of polyethylene glycol-coated hollow gold nanospheres. *Part Fibre Toxicol* 2014;**11**(26).